Author Manuscript

Author Manuscript

Author Manuscript

Author Manuscript

HHS Public Access

Author manuscript

J Biomed Mater Res A. Author manuscript; available in PMC 2019 September 01.

Published in final edited form as:

J Biomed Mater Res A. 2018 September ; 106(9): 2412–2423. doi:10.1002/jbm.a.36434.

Decellularization and characterization of a whole intervertebral disc xenograft scaffold

Austin Hensley[1], **Jess Rames**[1], **Victor Casler**[1], **Christopher Rood**[1], **Joshua Walters**[1], **Christopher Fernandez**[1], **Sanjitpal Gill**[1,2], and **Jeremy Mercuri**[1]

[1]Laboratory of Orthopaedic Tissue Regeneration & Orthobiologics, Department of Bioengineering, Clemson University, Clemson, SC

[2]Department of Orthopaedic Surgery, Medical Group of the Carolinas – Pelham, Spartanburg Regional Healthcare System, Greer, SC

Abstract

Intervertebral disc (IVD) degeneration is a multi-factor process that results in the physical destruction of the nucleus pulposus (NP) and annulus fibrosus (AF). This compromises IVD function and causes significant disability and economic burden. Strategies to replace the entire composite structure of the IVD are limited and most approaches do not recapitulate the heterogenous biochemical composition, micro-architecture or mechanical properties of the native tissue. Our central hypothesis was that donor IVDs which resemble the size and biochemistry of human lumbar IVDs could be successfully decellularized while retaining the tissue's structure and function with the long-term goal of creating a composite scaffold for tissue engineering the human IVD. Accordingly, we optimized a procedure to decellularize bovine tail IVDs using a combination of detergents, ultrasonication, freeze-thaw cycles, and nucleases. The resultant decellularized whole IVD xenografts retained distinct AF and NP regions which contained no visible intact cell nuclei and minimal residual bovine DNA (65.98±4.07 ng/mg and 47.12±13.22 ng/mg, respectively). Moreover, the NP region of decellularized IVDs contained 313.40±50.67 μg/mg glycosaminoglycan. The presence of collagen type II was confirmed via immunohistochemistry. Additionally, histological analysis of the AF region of decellularized IVDs demonstrated retention of the native angle-ply collagen micro-architecture. Unconfined compression testing demonstrated no significant differences in swelling pressure and toe-region modulus between fresh and decellularized IVDs. However, linear region moduli, peak stress and equilibrium moduli were all significantly reduced. Together, this research demonstrates a successful initial step in developing a biomimetic acellular whole IVD xenograft scaffold for use in IVD tissue engineering.

Key Terms

Intervertebral Disc; Xenograft; Decellularization; Tissue Engineering; Scaffold

Corresponding Author: Jeremy J. Mercuri, 313 Rhodes Engineering Research Center, Clemson University, Clemson, SC 29634, Phone: (864) 656-0978, Fax: (864) 656-4466.

Author Manuscript Author Manuscript Author Manuscript Author Manuscript

2. INTRODUCTION

Intervertebral discs (IVDs) are composite structures comprised of the nucleus pulposus (NP); a centralized fibro-gelatinous core of aggrecan and collagen type II, and the annulus fibrosus (AF); a multi-laminate, angle-ply structure of aligned type I collagen that circumferentially constrains the NP and anchors to adjacent vertebral end-plates. Due to its high fixed charge density, the NP generates an osmotic swelling pressure which is resisted in part by the AF via the generation of circumferentially directed tensile hoop stresses. Together, the mechanical characteristics of these structures enable the IVD to support compressive loads while endowing the spinal column with flexibility for carrying out activities of daily living. Unfortunately, nearly 5.7 million Americans are diagnosed with IVD disorders annually,[1] which include IVD degeneration; a multi-factor condition which results in the aberrant cell-mediated degradation of both NP and AF tissue in the IVD. As a consequence, normal spinal function is impaired resulting in altered kinematics,[2–4] low back pain,[5] and long-term disability that has an annual economic burden of $100B.[6] Thus restoration of the composite IVD structure and its function holds promise for significantly improving the quality of life for millions globally.

Current surgical strategies employed to mitigate the effects of IVD degeneration include spinal fusion and total disc arthroplasty.[7,8] The primary goal of these approaches is to relieve neurologic impingement via restoration of IVD height and spinal stability and to preserve spinal motion, respectively. Although these interventions may relieve the symptoms of IVD degeneration, they suffer from significant drawbacks including inducing adjacent segment degeneration in proximal IVDs,[9,10] and they do not recapitulate normal spinal biomechanics or the native composite architecture of the entire IVD.

Restoration and regeneration of the entire IVD with autografts/allografts or the development of whole-IVD scaffolds for tissue engineering the IVD are attractive alternatives to the use of artificial implants. Since the early 1990's studies have demonstrated the feasibility of implanting cryopreserved or fresh IVD allografts/autografts in a limited number of large animal and human trials.[11–15] While the structure of the IVDs and their mechanical function were reported to be preserved, the long-term metabolic activity and viability of the resident IVD cells was severely diminished or absent. Moreover, considering the significant number of individuals who exhibit evidence of IVD degeneration, donor supply of non-degenerate grafts is limited, and immunogenicity and resultant rejection remain a concern. Alternatively, researchers have begun to develop whole-IVD scaffolds with the long-term goal of tissue engineering and replacing the entire IVD.[16–20] These scaffolds often contain a hydrogel core and circumferentially-constraining casing, which attempt to mimic the NP and AF, respectively and support cellular viability and extracellular matrix (ECM) production.[18] However, these implants often fail to match the geometry and size, biochemistry, micro-architecture and mechanical characteristics of native human IVD tissue. This suggests a need for a revised approach for creating whole-IVD scaffolds.

Our group has previously reported on the development of top-down approach for creating acellular scaffolds for IVD repair and regeneration.[21–23] More specifically, a decellularization process was developed to create an acellular scaffold from excised bovine

Author Manuscript Author Manuscript Author Manuscript Author Manuscript

tail (coccygeal; CC) IVD NP tissue while concomitantly retaining the primary biochemical composition and ECM micro-architecture of the native tissue.[22] Bovine tail IVDs were chosen as a starting material for scaffold development because they have been shown to have similar biochemical composition, structural organization, resting stress and height to diameter ratio when compared to human lumbar IVDs.[24–26] Moreover, bovine tail IVDs are a readily available by-product of meat processing. Together, this suggests that bovine tail IVDs may be an optimal source for developing composite IVD scaffolds via decellularization if the native ECM can be maintained. Thus, expanding upon our initial success of decellularizing the NP region of bovine tail IVDs, the objective of the work herein was to define an optimized decellularization procedure which could be used to simultaneously decellularized both the NP and AF regions of whole bovine tail IVDs for their eventual use as a composite IVD xenograft scaffold. Moreover, we wanted to evaluate the observed changes in critical biochemical components, ECM micro-architecture and mechanical characteristics of the resulting decellularized construct compared to the starting material.

3. MATERIALS & METHODS

3.1 Bovine IVD isolation and decellularization

Fresh tails from 2–3-year-old cattle were obtained from a local grocer and stored at −20°C until isolation. After thawing at room temperature, tails were bathed in betadine to remove bacteria prior to removal of excess muscle and fat surrounding the functional spinal units. IVDs were visually located by flexing the tail joints and were dissected using a scalpel by cutting at the junction of the cartilaginous endplate of the IVD and the adjacent vertebral bodies. Whole IVDs were harvested from the three most cranial coccygeal levels (CC_{1-2}, CC_{2-3}, and CC_{3-4}) and were individually placed in 150 ml specimen containers. An equal number of IVDs from each level were included in the control (i.e. non-decellularized) and decellularized IVD groups to account for differences in spinal level. Control IVDs were stored at −20°C while the remaining IVDs underwent decellularization which included the use of a detergent-based solution comprised of 50 mM Tris Buffer (pH 7.5) containing 1.2% (v/v) Triton X-100, 0.2% (w/v) EDTA, and 0.02% (w/v) sodium azide. The step-wise decellularization process for whole bovine IVDs (Figure 1A) was as follows. Individual IVDs were placed at −80°C for two hours prior to the addition of 100ml of decellularization solution. IVDs were then thawed at room temperature within the decellularization solution on orbital shaker at 150RPM where they remained for a total of 22 hours. Subsequently, IVDs were ultrasonicated individually for 10 minutes at 42 kHz in the decellularization solution. IVDs were removed from decellularization solution and frozen again at −80°C. This process was repeated a total of three cycles (approximately 24 hours per cycle) using fresh changes of decellularization solution each cycle. After the third decellularization cycle, IVDs were rinsed in serial changes of distilled water (duration: 1 hour), 70% ethanol (duration: 30 minutes) and distilled water (duration: 30 minutes) again while under constant agitation at 150RPM on an orbital shaker at room temperature. After rinsing, each IVD was submerged in 100ml of 1x PBS (pH 7.5) containing with a solution containing 5 mM magnesium chloride and DNase/RNase (720 mU/mL each) at 37°C for 48 hours. Each nuclease treated IVD was rinsed twice for 30 minutes with two changes of 100 ml distilled

Author Manuscript Author Manuscript Author Manuscript Author Manuscript

water under agitation (150RPM) on an orbital shaker at room temperature. To sterilize the decellularized IVDs, each sample was submerged in 0.1% (v/v) solution of peracetic acid (pH 7.4) at room temperature on an orbital shaker at 150 rpm for two hours. A final rinse was then performed with changes of distilled water to remove residual peracetic acid.

3.2 Picogreen analysis for detection of residual double stranded bovine DNA

Axial, full thickness tissue samples were obtained via a 3mm-diameter biopsy punch from the central region of the NP (n=5) and four regions of the outer AF (anterior; n=5, posterior; n=5, left lateral; n=5, right lateral; n=5) of both control and decellularized IVDs. Samples were frozen at −80°C, lyophilized for 48 hours and dry weights recorded for data normalization. Samples were then completely digested in PBE buffer (pH 7.5) containing 5 mM L-Cysteine, 100 mM dibasic phosphate buffer, and 5 mM EDTA and 125 μg/mL papain at 65°C for 24 hours. Digested samples were diluted and assayed in black-walled 96-well plates according to manufacturer's instructions. Fluorescence was detected using an excitation wavelength of 480 nm and an emission wavelength of 520 nm. Double stranded DNA content was determined from a standard curve developed from known concentrations of DNA supplied by the manufacturer and expressed as ng/mg dry weight.

3.3 Agarose gel electrophoresis for detection of residual bovine DNA

Aliquots of biopsy sample digests described above for PicoGreen analysis were evaluated via agarose gel electrophoresis. Briefly, digests underwent DNA purification using a Qiagen Dneasy® Blood and Tissue extraction kit according to manufacturer's instructions. Purified DNA samples (20μl) were loaded into wells of both 1% (w/v) and 5% (w/v) agarose gels made with Tris-Boric acid-EDTA buffer and containing ethidium bromide from both control and decellularized samples in conjunction with high (300–24,000bp) and low (10–300bp) molecular weight DNA ladders, respectively. Gels were run at 100V for 60 minutes and were imaged using a bio-imager system (Bio-Rad) with an ethidium bromide filter to detect DNA bands.

3.4. Ethidium staining for detection of residual bovine DNA

Cylindrical biopsy samples from the NP, transition zone/inner AF, and outer AF were obtained as described above from both control (n=3) and decellularized (n=3) bovine IVDs. Samples were placed in a solution of 2 mM ethidium homodimer-1 in PBS for 30 min. Samples were then thinly sectioned using a scalpel blade and imaged with a Zeiss AxioVertA.1 fluorescent microscope.

3.5. Quantitative evaluation of bovine IVD glycosaminoglycan content

Aliquots of biopsy sample digests described above for PicoGreen analysis were evaluated via dimethylmethylene blue (DMMB) assay. Briefly, fresh control and decellularized NP samples were diluted 1000X and 200X in PBE buffer respectively. Additionally, fresh control and decellularized AF samples were diluted 200x and 100x, respectively. Fifty microliters of each diluted sample were assed in duplicate with 200ul of DMMB reagent (40 mM sodium chloride, 40 mM glycine 46 μM DMMB; pH: 3.0) in a 96-well plate.

Author Manuscript Author Manuscript Author Manuscript Author Manuscript

Absorbance was read at a wavelength of 525nm and GAG content was determined from a standard curve containing known concentrations of chondroitin-6-sulfate.

3.5. Histological sample preparation

Control and decellularized bovine IVD samples were fixed in 10% neutral buffered formalin prior to bisecting the samples in the mid-transverse (axial) plane in order to visualize a full-thickness cross-section of the NP and AF regions. Samples were subsequently equilibrated in a 15% (w/v) sucrose solution overnight at 4°C followed by equilibration in a 30% (w/v) sucrose solution for 2 hours. Samples were then transferred to a solution containing 50:50 solution of 30% (w/v) sucrose in 1x PBS and Optimum Cutting Technology (OCT) polymer for 2 hours under agitation (150RPM) at room temperature. The cut surface of the tissue samples was placed face-down in cryo-molds, filled with 100% OCT and stored at −80°C. Sample sections of 8-micron thickness were obtained using a cryotome, placed on positively charged slides and stored at −20°C until staining.

3.6 Histological and immunohistochemical evaluation of bovine IVD ECM biochemistry and micro-architecture

To qualitatively compare glycosaminoglycan content of NP and AF regions of control (n=5) and decellularized (n=5) bovine IVDs, cryo-sections were mordant in 3% (v/v) aqueous acetic acid followed by staining with 1% (v/v) Alcian blue in 3% acetic acid (pH 2.5) and 0.1% (w/v) nuclear fast red. To qualitatively compare proteoglycan content of the NP and AF regions of control and decellularized bovine IVDs, additional cryo-sections were stained with a 1% (w/v) Safranin-O solution containing 1% (v/v) glacial acetic acid in PBS and 0.02% (w/v) fast green solution. To qualitatively evaluate collagen content of the NP and AF regions of control and decellularized bovine IVDs, additional cryo-sections were stained initially with Wiegert's hematoxylin followed by Picrosirius red solution (Poly Scientific). To visualize collagen fiber alignment in the tissue sections, polarized light microscopy was utilized. Additionally, to quantitatively compare fiber alignment within decellularized and fresh bovine AF tissue, histological sections were obtained at an oblique angle using a previously described method.[23] The fiber alignment relative to the interface between adjacent lamellae was determined using the angle measurement tool in NIH Image-J software. Fifteen total measurements were obtained from three different images (n = 5 measurements/image) taken using a polarizing lens at 100x total magnification for both fresh and decellularized AF tissue. Average fiber angle was determined and compared between groups.

The presence of collagen type II in the NP and AF regions of control (n=3) and decellularized (n=3) bovine IVDs was determined via immunohistochemistry. Briefly, tissue sections were fixed in cold acetone for 15 minutes. Non-specific antibody binding and endogenous peroxidases were blocked using a solution of 0.3% (v/v) normal goat serum containing 0.3% (v/v) hydrogen peroxide in tris buffered saline. Slides were incubated in an anti-bovine collagen type II rabbit polyclonal antibody (Abcam – ab78482; 1:50 dilution) for 30 minutes at room temperature prior to thorough rinsing and incubation with a secondary biotinylated antibody and avidin-biotin complex according to manufacturer's instructions (Vectastain® ABC Kit Rabbit IgG – Vector Labs) for 30 minutes. A DAB

Author Manuscript Author Manuscript Author Manuscript Author Manuscript

substrate kit (Vector Labs: SK4100) was used according to manufacturer's instructions in conjunction with counterstaining in diluted hematoxylin to visualize positive IHC staining and cell nuclei, respectively. All histological images were captured at 100x and 200x total magnification using a Zeiss AxioVertA.1 microscope and AxioVision SE64 Rel. 4.9.1 software.

3.7 Unconfined compression testing of bovine IVDs

Due to swelling of the NP and inner AF of decellularized bovine IVDs, osmotic compaction was performed prior to unconfined compression testing. Prior to compaction, the cross-sectional area of the swollen NP and inner AF was determined via digital calipers. Compaction was then achieved by securing decellularized IVDs in 12–14kDa MWCO dialysis tubing containing 50mM MES buffer and submersion in 20kDa polyethylene glycol (0.2546g/ml MES generating approximately 1MPa of osmotic pressure)[27] at room temperature for up to 72 hours until original IVD height was achieved.

For unconfined compression testing, control (n=5) and compacted/decellularized (n=5) IVDs were tested using an Instron test frame fitted with a 500N load cell and clear plexiglass tank filled with saline and protease inhibitor (25°C). Samples were initially preloaded to 1N of compression, digital images of initial IVD widths were recorded, and sample heights were determined from actuator displacement. Sample heights were used to track and calculate the applied strain for the remainder of testing. Samples were subsequently allowed to swell under the compression platen for 24 hours until equilibrium was reached. During this time the test frame tracked and recorded the peak swelling load which was later divided by the original swollen cross-sectional area of the NP and inner AF prior to osmotic compaction. Following swelling, a digital image of the IVD width was captured which was subsequently used to calculate cross-sectional area. Next the IVD samples immediately underwent multicycle compression testing to 12% strain at 1 mm/min for a total of 10 cycles. The final force-displacement curve was normalized to the original cross-sectional area for each sample. Toe and linear region moduli was determined from the slope of the stress-strain curves between 2–4% and 10–12% applied strain, respectively. Immediately after multi-cycle compression testing (preconditioning), samples underwent incremental stress relaxation testing to a final axial strain of 12% (based on initial sample heights) using 4% strain increments applied at 4%/second; with each strain level being held until equilibrium was reached (defined as no change in load greater than 0.01N over a 30 second period). Digital images of sample widths were captured immediately after the application of each incrementally applied strain and at equilibrium in order to calculate the IVD area (determined by assuming the IVD maintained a circular cross-sectional area and using the width as the diameter) at these points during testing. Image-J software was used to measure sample widths from captured images. Peak stress was determined at each increment by dividing the peak force by IVD cross-sectional area. Equilibrium modulus was calculated by dividing the equilibrium stress by the respective applied strain. Percent change in radial expansion was calculated as $(D_{swell} - D_{12\%Eq})/(D_{swell})] \times 100$, where D_{swell} is the diameter of the IVD measured after equilibrium swelling testing and $D_{12\%Eq}$ is the IVD diameter measured at equilibrium following the application of 12% strain during stress relaxation testing.

Author Manuscript Author Manuscript Author Manuscript Author Manuscript

3.8 Statistics

All quantitative data is expressed as a mean ± standard error of the mean (SEM). Statistical comparisons between control and decellularized samples using a Student's T-test of equal variance with significance defined as $p \leq 0.05$. Statistical analysis of the data was performed using GraphPad Prism 7 software.

4. RESULTS

4.1 Decellularized whole bovine tail intervertebral discs retain distinct AF and NP gross morphology

A combination of detergents, ultrasonication and freeze-thaw cycles, and nucleases were used to decellularize fresh whole bovine tail IVD samples (Figure 1A). The average height and diameters of the IVDs (Figures 1B&C) were 6.69±1.25 mm and 21.81±1.39 mm, respectively. Following decellularization, fresh bovine tail IVD tissue transitioned from a fleshy red color to gleaming white (Figure 1D&E). Additionally, the NP and inner AF regions became swollen and projected cranially from the outer AF. These regions were distinguishable from each other as the NP appeared as a glossy white firm hydrogel which transitioned to a fibrous inner AF surrounded by circumferentially oriented collagenous lamellae in the outer AF (Figure 1E). The swollen NP and inner AF could be osmotically compacted back within the confines of the outer AF following placement of the decellularized whole IVD in dialysis tubing and submersion for approximately 18-hours in a polyethylene glycol solution that generated 1MPa of osmotic pressure (Figures 1F–H). As a result, the IVD was restored to its original, non-swollen configuration achieving the pre-decellularized sample height (Figure 1I). Of note, the compacted decellularized IVD could re-swell within 2 hours upon re-immersion in physiologic saline (data not shown).

4.2 Decellularized whole bovine tail intervertebral discs contain no intact cell nuclei or DNA

To determine the efficacy of the decellularization process on whole bovine tail IVDs, DNA quantification, electrophoresis and histological analyses for residual DNA and cell nuclei were performed on tissue samples from both the NP and AF regions of decellularized IVDs compared to fresh samples. The average DNA content of the AF and NP regions of fresh bovine IVDs was 244.70±25.68 ng/mg and 286.7±43.86 ng/mg, respectively (Figure 2A&B). These values were significantly reduced to 65.98±4.07 ng/mg ($p<0.001$) and 47.12±13.22 ng/mg ($p<0.001$) resulting in a 73% and 84% decrease in AF and NP tissue DNA content, respectively (Figure 2A&B). Electrophoresis on purified DNA samples isolated from AF and NP regions of fresh IVDs ran on 1% (Figure 2C&D) and 5% (Figure 2E&F) agarose gels demonstrated the presence of intact, high molecular weight DNA. Conversely, samples from the AF and NP region of decellularized whole bovine IVDs illustrated the complete absence of both high and low molecular weight DNA, respectively. Furthermore, ethidium staining performed on AF, transition zone, and NP tissue samples from fresh bovine tail IVDs (Figures 2G, H & I, respectively) demonstrated the presence of morphologically distinct intact cell nuclei and nucleic acid in each respective region. Similar staining was absent in the respective tissue regions of decellularized whole IVDs (Figure 2J, K & L).

Author Manuscript Author Manuscript Author Manuscript Author Manuscript

4.3 Decellularized whole bovine tail intervertebral discs retain GAG

The effect of decellularization on extracellular matrix GAG content of bovine tail IVDs was quantified biochemically and qualitatively analyzed via histology using tissue samples extracted from both the AF and NP regions of fresh and decellularized whole IVDs. Average GAG content of AF and NP regions of fresh IVDs was 224.60±23.91 μg/mg and 569.70±99.93 μg/mg, respectively (Figure 3A&B). Average GAG concentrations in the AF (96.93±18.46 μg/mg) and NP (313.40±50.67 μg/mg) of decellularized whole bovine tail IVDs were significantly reduced ($p=0.0013$ and $p=0.041$, respectively) compared to respective fresh values. Thus, decellularization resulted in a 56.84% and 45.00% reduction in AF and NP GAG content, respectively. Histological analysis of alcian blue stained fresh AF (Figure 3C&E) illustrated intact cell nuclei populating a fibrous matrix that stained predominantly pink with light blue GAG staining found interspersed within the fibers of the lamellar architecture and within the interlamellar matrix. Fresh NP (Figure 3D&F) stained intensely blue indicating a GAG-rich matrix that was sparsely populated throughout with round cell nuclei residing within lacunae-like structures. Following decellularization, all staining was considerably lighter throughout the entire AF and no cell nuclei were visible (Figure 3G). Decellularized NP demonstrated lighter blue staining compared to fresh tissue indicative of a reduction in GAG content; however, much of the matrix micro-architecture of the decellularized NP was retained with no intact cell nuclei visible (Figure 3H).

4.4 Decellularized whole bovine tail intervertebral discs retain AF and NP micro-architecture

To confirm the maintenance of the distinct AF- and NP- micro-architecture within the decellularized whole bovine IVDs, histology was performed. H& E staining of fresh AF (Figures 4A&E) illustrate a multi-lamellar architecture containing numerous cell nuclei. Safranin-O staining of fresh AF (Figures 4I&M) illustrated the presence of interlamellar GAG which increased in staining intensity from outer AF to inner AF. H&E staining of fresh NP (Figures 4C&G) illustrate a homogenous matrix containing round cell nuclei interspersed within. Safranin-O staining of fresh NP (Figures 4K&O) stained intensely for GAG and illustrated the presence of small fibers randomly aligned throughout.

Following decellularization, the lamellar and interlamellar regions of the AF were devoid of cells and stained less intensely with H&E (Figures 4B&F) and safranin-O (Figures 4J&N) indicating disruption/loss of matrix components. However, the lamellar and interlamellar regions were clearly visible indicating that the micro-architecture was retained. Similarly, H&E (Figures 4D&H) and safranin-O (Figures 4L&P) staining of the NP was less intense following decellularization, however the amorphous appearance of the tissue was retained.

4.5 Decellularized whole bovine tail intervertebral discs retain collagen organization

To determine the retention and organization of collagen within the decellularized whole bovine IVDs, IHC for collagen type II and picrosirius red staining with polarized-light microscopy was performed. Expectedly, collagen type II was absent in the fresh (Figure 5A) and decellularized (Figure 5B) AF. However, picrosirius red staining indicated that intact collagen fibers (likely collagen type I) were observed in the decellularized AF. These fibers were found in an angle-ply orientation within lamellae and demonstrated a fiber-preferred

Author Manuscript Author Manuscript Author Manuscript Author Manuscript

alignment (Figures 5E&I) and birefringent fiber crimp (Figures 5F&J). Image analysis of decellularized AF histological sections demonstrated an average fiber angle of 34.40°±1.52° which alternated in direction in adjacent lamellae. This was not significantly different compared to the fiber angles measured in fresh AF (37.23°±2.01°). Decellularized NP demonstrated diffuse staining for collagen type II (Figure 5C&D) within a matrix containing sparse matrix fibers (Figures 5G&H). Polarized light microscopy confirmed the presence of small collagen fibers which were randomly oriented throughout the NP matrix (Figures 5K&L).

4.6 Decellularized whole bovine tail intervertebral discs have reduced unconfined compressive mechanical properties

To determine the effect of decellularization on whole bovine IVD mechanical properties, equilibrium swelling, cyclic compression, and unconfined incremental compressive stress relaxation testing was performed on fresh and decellularized whole bovine IVDs. Representative images depicting mechanical testing of fresh and decellularized whole bovine IVDs are shown in Figures 6A&B, respectively. Representative cyclic compressive (Figure 6C) and incremental stress relaxation testing (Figure 6D) curves from fresh whole bovine IVDs demonstrated higher magnitudes of stress and load, given the same applied strains compared to decellularized whole bovine IVDs (Figures 6E&F, respectively). Average time to relaxation during incremental stress relaxation testing also tended to be longer for fresh whole bovine IVDs compared to decellularized samples. The swelling pressure generated by fresh IVDs (0.043±0.030 MPa) tended to be greater compared to decellularized IVDs (0.006±0.002 MPa) however, this was not found to be significant ($p=0.148$) (Figure 6G). Toe-region modulus determined from multi-cycle compression testing tended to be higher for fresh bovine IVDs (0.828±0.464MPa) compared to decellularized (0.134±0.048MPa), however this difference was not significant ($p=0.09$). Linear-region modulus was significantly greater ($p=0.010$) for fresh whole bovine IVDs (10.132±3.765MPa) compared to decellularized samples (0.640±0.360 MPa), respectively (Figure 6G). Similarly, average peak stress and equilibrium moduli at 4%, 8%, and 12% strain for fresh whole bovine IVDs were 6- to 10-times greater ($p=0.035$, $p=0.008$, $p=0.003$, and $p=0.046$, $p=0.021$, $p=0.01$, respectively) compared to decellularized samples tested to the same applied strain end-points (Figure 6G). Both sample types exhibited an average peak stress that increased with increasing applied strains, whereas the opposite trend was found for their equilibrium moduli (Figure 6G). Percent increase in radial expansion trended towards being lower in decellularized whole bovine IVDs (3.016±1.485%) as compared to fresh controls (6.202±2.532%), however this difference was not found to be statistically significant.

5. DISCUSSION

Herein we have defined a scalable decellularization procedure that effectively removes cell nuclei and residual DNA from both the NP and AF regions of whole bovine tail IVDs. The resulting composite structure, although swollen, had the same morphologically distinct regions (i.e. NP and AF), primary ECM components and micro-architecture as has been observed in human lumbar IVDs. While significant reductions in NP GAG, swelling

Author Manuscript Author Manuscript Author Manuscript Author Manuscript

pressure and unconfined compressive properties were noted in decellularized whole bovine IVDs as compared to fresh tissue, the composite structures were osmotically responsive, mechanically competent, and able to resist unconfined compressive loading. Taken together, this work represents the initial steps towards developing an acellular composite scaffold for use in regenerating the IVD in its entirety.

The primary objective of decellularizing allogenic or xenogenic tissues for the creation of biomaterial scaffolds is to remove all cells, nuclear material and antigenic epitopes while maintaining critical ECM components, their spatial distribution, relative ratios, and tissue micro-architecture.[22,28–38] This top-down approach to scaffold development aims to minimize the possibility of immune rejection while yielding a biomimetic scaffold that can promote targeted tissue regeneration. Moreover, this approach offers several advantages compared to building scaffolds from the ground-up including; 1) obtaining a 'pre-fabricated,' tissue-specific micro-architecture without employing complex additive manufacturing techniques, which 2) yields scaffolds that provide 'built-in' instructional cues to local/seeded cells instructing them to attain tissue-specific phenotypes and contribute to tissue regeneration even in the absence of other exogenous soluble growth and differentiation factors.[38,39]

Several tissues have been successfully decellularized via chemical detergents and physical methods for the purpose of creating biomimetic scaffolds.[37] However, most of the tissues are thin allowing for easy diffusion of detergents throughout the ECM structure. Our goal was to develop a decellularization process that yields an acellular whole IVD scaffold; a tissue that is relatively thick, has a low surface area to volume ratio and is composed of multiple tissue types with appreciably different biochemical compositions and micro-architectures. We chose to use a multicomponent, detergent-based decellularization solution coupled with ultrasonication and freeze-thaw cycles. The non-ionic detergent Triton X-100 in conjunction with ethylenediaminetetraacetic acid (EDTA) was used to permeabilize and release cells from the IVD ECM while minimizing charge-based interactions with the IVD GAG content. Repeated freeze-thaw and ultrasonication cycles were also employed to disrupt cell membranes via the generation of ice crystals and mechanical shockwaves to 'loosen' the ECM to improve detergent diffusion. Subsequent rinses in nucleases and changes of distilled water and 70% ethanol degraded any residual bovine DNA/RNA and allowed for sequential swelling and dehydration of the IVD ECM creating a 'bellows-like' ebb and flow of fluid to facilitate cell component and precipitated nucleic acid removal, respectively.

Our group is not the first to attempt to overcome the challenge associated with decellularizing a whole IVD. Chan et al reported the ability to partially decellularize whole bovine tail IVDs using a combination of 0.1% sodium dodecylsulfate (SDS) in phosphate buffered saline containing 1x EDTA and multiple freeze-thaw cycles over a 48-hour time period.[35] This resulted in complete devitalization of IVD cells, removal of 71% and 76% of intact cell nuclei from the NP and AF regions, respectively while maintaining near-native levels of IVD GAG content.[35] However significant differences exist between their work and the work herein. First, Chan's bovine tail IVD tissue was obtained from the CC_{4-5} to CC_{10-11}-disc spaces which are roughly 1/2 the size of the CC_{1-2} to CC_{3-4} IVDs used herein. This likely allowed for the use of significantly shorter decellularization times as compared to

Author Manuscript Author Manuscript Author Manuscript Author Manuscript

the protocol used herein. Additionally, considering the larger size of the IVDs, we chose to remove the cartilaginous endplates to allow for swelling of the NP and inner AF tissue to facilitate efficient diffusion of the detergents from all sides of the tissue. Finally, we exhaustively evaluated the decellularized composite structures for residual DNA content using numerous quantitative biochemical methodologies as opposed to semi-quantitative histology as was reported previously. Taken together, our work herein represents a novel approach to decellularizing large IVDs that more closely approximate the size and geometry of the human lumbar IVDs while performing an in-depth characterization of the resultant construct's biochemical, histological/micro-architectural and compressive mechanical characteristics.

Acceptance criteria for successful tissue decellularization have been defined previously by others.[36,37] These benchmarks include the absence of visible cell nuclei via hematoxylin and eosin histological staining and residual DNA content of ≤ 50ng/mg. These criteria must be met to minimize a potential immunological host response to the construct. Herein, we have demonstrated the combined average residual DNA content of NP and AF regions meet this criterion. Additionally, we have demonstrated the absence of residual DNA between 10 – 24,000 bp via agarose gel electrophoresis and tissue section staining with ethidium.

In addition to successfully removing bovine DNA, the decellularization process employed herein resulted in the retention of GAG and collagen type II within the NP region of the decellularized whole bovine IVDs. Chondroitin sulfate is the predominant GAG found within the human NP and is often found as a part of the larger proteoglycan aggrecan.[40] Collagen type II is the most abundant collagen isoform found in native NP tissue which forms a loose fiber network with other minor collagens, including type IX and XI which together help to restrain swelling of aggrecan.[41] The average GAG content of normal NP ranges from 500-800ug/mg dry weight,[42] and is found in a ratio of 27:1 with collagen in normal NP tissue.[43] By comparison, mildly degenerative IVDs display an average GAG content of ~250ug/mg dry weight in the NP.[44] Herein, we demonstrated that fresh bovine tail NP demonstrated similar GAG content to normal human NP tissue. Expectedly, the decellularized whole bovine IVDs NP demonstrated reduced GAG content which likely resulted from swelling and leaching of these molecules from the ECM during decellularization. In fact, others have demonstrated that GAG leaching readily occurs from tissues when merely placed in aqueous solutions if they are not chemically stabilized.[45] However, the retained GAG content of the decellularized intact bovine IVDs resembles that of a mildly degenerate IVD and is comparable or greater than that found in other NP scaffolds.[22,34,46–48] Additionally, we have demonstrated via IHC and polarized light microscopy that a network of collagen type II is retained within the NP region of the decellularized IVDs similar to that found in native human NP tissue.

It was also found that the biochemical composition and highly organized micro-architectural structure of the AF region of the whole bovine IVD was also retained following decellularization. The native AF of human lumbar IVDs is an anisotropic structure that is composed of the outer AF and inner AF. The outer AF is comprised of 12–25 concentric sheets, or lamellae, of type I collagen with interlamellar GAG and trans-lamellar fiber elements interposed between the layers.[49–52] Moreover, the predominant collagen fiber

Author Manuscript Author Manuscript Author Manuscript Author Manuscript

alignment of the outer AF alternates ±28–43° to the horizontal axis of the spinal column within each subsequent lamella giving rise to an 'angle-ply architecture.'[53] The defined lamellae of the outer AF gradually become less distinguishable as you transition radially inwards to the inner AF. During this transition which is attributable to ECM produced by distinct cell phenotypes in the AF,[54] the collagen type I content decreases and collagen type II and proteoglycan increases. It was clearly evident that the AF region of fresh bovine IVDs demonstrated a gross anatomical heterogeneity comparable to human lumbar IVDs having a fibrous and defined outer AF which eventually transitioned to a fibro-gelatinous inner AF. During decellularization, cranially-directed swelling of the NP and inner AF/transition zone was evident which helped to delineate the inner and outer AF respectively. Histologically, fresh bovine AF demonstrated a multi-laminate, angle-ply architecture with the presence of interlamellar GAG. Following decellularization of the whole bovine IVD, interlamellar GAG was reduced and AF lamellar thickness tended to increase. The former observation was likely due in part to ultrasonication which has been shown to be an effective method for decellularizing dense fibrous tissues by loosening fiber networks.[21] However, recent studies by our group have demonstrated that this loosening can be beneficial for supporting increased cell infiltration without significantly impacting tensile strength of multi-laminate angle-ply biomaterials.[21] Moreover, the overall angle-ply lamellar architecture, collagen fiber network and alignment of the native outer AF was retained in the decellularized whole bovine IVDs.

Another significant finding from this work was that the NP region of the decellularized whole bovine IVD retained an osmotic potential and demonstrated the ability to swell in physiologic saline when confined axially under a compression platen and circumferentially by the AF. This is one of the mechanisms by which the native NP in human IVDs resists compressive loads that arise during activities of daily living. More specifically, the aggrecan-rich isotropic ECM of the NP generates an osmotic potential due to its high fixed charge density which draws water into the tissue causing it to swell in an unloaded state.[40] Upon compressive loading, an intradiscal hydrostatic pressure is generated due to induced fluid flow and low permeability of the NP limiting water exudation. Together with the modulus of the NP ECM, these mechanisms provide the primary resistance to applied compressive loads. Under passive loading due to body weight and stabilizing forces developed by the paraspinal musculature, the confined NP equilibrium intradiscal swelling pressure in the normal lumbar IVD is approximately 0.1MPa,[53,55] which has been shown to decrease to 0.03MPa in mildly degenerate IVDs.[56] Herein, we demonstrated that the native bovine tail IVD NP generated an equilibrium swelling pressure of approximately 0.05MPa which was reduced to 0.006MPa after decellularization. This reduction is likely the result of a combination of GAG lost during the decellularization procedure coupled with increased permeability of the decellularized ECM. Additionally, these lower values could be due to the fact that the whole bovine IVD samples tested were less constrained circumferentially as compared to the NP *in vivo. In vivo* the AF is anchored to adjacent vertebra which can limit the IVDs outward expansion, however the decellularized whole bovine IVDs lack vertebral bodies.

Finally, we found that although the magnitude of the overall compressive mechanical response of fresh and decellularized whole bovine IVDs were different, their qualitative

Author Manuscript Author Manuscript Author Manuscript Author Manuscript

characteristics (i.e. shape of the resultant testing curves and trends in mechanical response to the application of varying strain magnitudes) were similar. Additionally, both decellularized whole bovine tail IVDs and fresh controls exhibited the ability to radially expand with the application of increasing axial strain, however the former tended to expand less. This mechanical interaction resembles the phenomenon which occurs in the native human IVD whereby compressive loading of the IVD leads to pressurization of the NP which subsequently induces radially-directed compressive loading the AF. These radially-directed pressures compress the AF lamellae and interlamellar GAG preventing in-ward buckling and shearing of the lamellae and contributing to overall compressive stiffness of the IVD.[52] Thus the observed GAG loss from decellularization may have also accounted for the trend towards lower radial expansion in addition to compressive property magnitudes that were on the lower end of values reported for human IVDs.[57] Regardless, together the data suggests that the coordinate mechanical interactions between the NP and AF still exist following decellularization in the whole bovine IVDs. Ongoing work by our group aims to further enhance the compressive characteristics of the decellularized whole bovine IVD xenograft scaffold by re-introducing exogenous GAG into the NP region in addition to optimizing a chemical crosslinking protocol. Furthermore, considering the long-term goal of tissue engineering a complete IVD, seeding methods are being optimized to repopulate the decellularized whole bovine IVD scaffolds with human mesenchymal stem cells.

6. CONCLUSIONS

In conclusion, a simple and scalable decellularization procedure has been developed to yield a decellularized whole bovine IVD xenograft. Resultant acellular constructs biochemically, structurally and mechanically resemble the complex heterogeneity of the native IVD and represent an excellent starting point for developing tissue engineered whole IVD constructs for use in patients suffering from IVD degeneration.

Acknowledgments

Research support for the Ortho-X lab and this research has been provided in part by the Clemson University Creative Inquiry Program and the National Institute of General Medical Sciences of the National Institutes of Health (award number: 5P02GM103444). The authors would also like to acknowledge all past and present undergraduate creative inquiry students for their help in collecting data for this manuscript. We would also like to thank the Institute for Biological Interfaces of Engineering at Clemson for allowing us to use their Instron.

References

1. An HS, Thonar EJ-MA, Masuda K. Biological repair of intervertebral disc. Spine (Phila Pa 1976). 2003; 28(15 Suppl):S86–92. [PubMed: 12897480]
2. Rohlmann A, Zander T, Schmidt H, Wilke H-J, Bergmann G. Analysis of the influence of disc degeneration on the mechanical behaviour of a lumbar motion segment using the finite element method. J Biomech. 2006; 39(13):2484–2490. [PubMed: 16198356]
3. O'Connell GD, Vresilovic EJ, Elliott DM. Human intervertebral disc internal strain in compression: The effect of disc region, loading position, and degeneration. J Orthop Res. 2011; 29(4):547–555. [PubMed: 21337394]
4. Inoue N, Espinoza Orías AA. Biomechanics of Intervertebral Disk Degeneration. Orthop Clin North Am. 2011; 42(4):487–499. [PubMed: 21944586]
5. Mosley GE, Evashwick-Rogler TW, Lai A, Iatridis JC. Looking beyond the intervertebral disc: the need for behavioral assays in models of discogenic pain. Ann N Y Acad Sci. Aug.2017

Author Manuscript Author Manuscript Author Manuscript Author Manuscript

6. Risbud MV, Shapiro IM. Role of cytokines in intervertebral disc degeneration: pain and disc content. Nat Rev Rheumatol. 2014; 10(1):44–56. [PubMed: 24166242]
7. Ghiselli G, Wang JC, Bhatia NN, Hsu WK, Dawson EG. Adjacent segment degeneration in the lumbar spine. J Bone Joint Surg Am. 2004; 86-A(7):1497–1503. [PubMed: 15252099]
8. van Ooij A, Oner FC, Verbout AJ. Complications of artificial disc replacement: a report of 27 patients with the SB Charité disc. J Spinal Disord Tech. 2003; 16(4):369–383. [PubMed: 12902953]
9. Kim HJ, Kang KT, Chun HJ, Lee CK, Chang BS, Yeom JS. The influence of intrinsic disc degeneration of the adjacent segments on its stress distribution after one-level lumbar fusion. Eur Spine J. 2015; 24(4):827–837. [PubMed: 25022861]
10. Celestre PC, Montgomery SR, Kupperman AI, Aghdasi B, Inoue H, Wang JC. Lumbar clinical adjacent segment pathology: Predilection for proximal levels. Spine (Phila Pa 1976). 2014; 39(2): 172–176. [PubMed: 24153168]
11. Luk KD, Ruan DK, Chow DH, Leong JC. Intervertebral disc autografting in a bipedal animal model. Clin Orthop Relat Res. 1997; 337:13–26.
12. Luk KDK, Ruan DK, Lu DS, Fei ZQ. Fresh frozen intervertebral disc allografting in a bipedal animal model. Spine (Phila Pa 1976). 2003; 28(9):864–9. discussion 870. [PubMed: 12941999]
13. Luk KDK, Ruan DK. Intervertebral disc transplantation: A biological approach to motion preservation. Eur Spine J. 2008; 17(SUPPL 4):504–510. [PubMed: 19005699]
14. Matsuzaki H, Wakabayashi K, Ishihara K, Ishikawa H, Ohkawa A. Allografting intervertebral discs in dogs: a possible clinical application. Spine (Phila Pa 1976). 1996; 21(2):178–183. [PubMed: 8720401]
15. Ruan D, He Q, Ding Y, Hou L, Li J, Luk KD. Intervertebral disc transplantation in the treatment of degenerative spine disease: a preliminary study. Lancet. 2007; 369(9566):993–999. [PubMed: 17382826]
16. Choy ATH, Chan BP. A Structurally and Functionally Biomimetic Biphasic Scaffold for Intervertebral Disc Tissue Engineering. PLoS One. 2015; 10(6):e0131827. [PubMed: 26115332]
17. Xu B, Xu H, Wu Y, et al. Intervertebral disc tissue engineering with natural extracellular matrix-derived biphasic composite scaffolds. PLoS One. 2015; 10(4):1–16.
18. Yang Q, Xu H wei, Hurday S, Xu B shan. Construction Strategy and Progress of Whole Intervertebral Disc Tissue Engineering. Orthop Surg. 2016; 8(1):11–18. [PubMed: 27028376]
19. Moriguchi Y, Mojica-Santiago J, Grunert P, et al. Total disc replacement using tissue-engineered intervertebral discs in the canine cervical spine. PLoS One. 2017; 12(10):1–18.
20. Bowles RD, Gebhard HH, Hartl R, Bonassar LJ. Tissue-engineered intervertebral discs produce new matrix, maintain disc height, and restore biomechanical function to the rodent spine. Proc Natl Acad Sci. 2011; 108(32):13106–13111. [PubMed: 21808048]
21. Borem R, Madeline A, Walters J, Mayo H, Gill S, Mercuri J. Angle-ply biomaterial scaffold for annulus fibrosus repair replicates native tissue mechanical properties, restores spinal kinematics, and supports cell viability. Acta Biomater. 2017; 58:254–268. [PubMed: 28587986]
22. Fernandez C, Marionneaux A, Gill S, Mercuri J. Biomimetic nucleus pulposus scaffold created from bovine caudal intervertebral disc tissue utilizing an optimal decellularization procedure. J Biomed Mater Res - Part A. 2016; 104(12)
23. McGuire R, Borem R, Mercuri J. The fabrication and characterization of a multi-laminate, angle-ply collagen patch for annulus fibrosus repair. J Tissue Eng Regen Med. 2017; 11(12):3488–3493. [PubMed: 27943659]
24. Oshima H, Ishihara H, Urban JP, Tsuji H. The use of coccygeal discs to study intervertebral disc metabolism. J Orthop Res. 1993; 11(3):332–338. [PubMed: 8326439]
25. Alini M, Eisenstein SM, Ito K, et al. Are animal models useful for studying human disc disorders/degeneration? Eur Spine J. 2008; 17(1):2–19. [PubMed: 17632738]
26. Perie DS, Maclean JJ, Owen JP, Iatridis JC. Correlating material properties with tissue composition in enzymatically digested bovine annulus fibrosus and nucleus pulposus tissue. Ann Biomed Eng. 2006; 34(5):769–777. [PubMed: 16598654]
27. Urban JP, McMullin JF. Swelling pressure of the lumbar intervertebral discs: influence of age, spinal level, composition, and degeneration. Spine (Phila Pa 1976). 1988; 13(2):179–187. [PubMed: 3406838]

Author Manuscript Author Manuscript Author Manuscript Author Manuscript

28. Huang Z, Kohl B, Kokozidou M, Arens S, Schulze-Tanzil G. Establishment of a Cytocompatible Cell-Free Intervertebral Disc Matrix for Chondrogenesis with Human Bone Marrow-Derived Mesenchymal Stromal Cells. Cells Tissues Organs. 2016; 201(5):354–365. [PubMed: 27160711]
29. Illien-Jünger S, Sedaghatpour DD, Laudier DM, Hecht AC, Qureshi SA, Iatridis JC. Development of a bovine decellularized extracellular matrix-biomaterial for nucleus pulposus regeneration. J Orthop Res. 2016; 34(5):876–888. [PubMed: 26509556]
30. Xu H, Xu B, Yang Q. , et al. Comparison of Decellularization Protocols for Preparing a Decellularized Porcine Annulus Fibrosus Scaffold. In: Pandit A, editorPLoS One. Vol. 9. 2014. e86723
31. Lin X, Fang X, Wang Q, et al. Decellularized allogeneic intervertebral disc: natural biomaterials for regenerating disc degeneration. Oncotarget. 2016; 7(11):12121–12136. [PubMed: 26933821]
32. Wachs RA, Hoogenboezem EN, Huda HI, Xin S, Porvasnik SL, Schmidt CE. Creation of an injectable in situ gelling native extracellular matrix for nucleus pulposus tissue engineering. Spine J. 2017; 17(3):435–444. [PubMed: 27989725]
33. Wu L-C, Kuo Y-J, Sun F-W, et al. Optimized decellularization protocol including α-Gal epitope reduction for fabrication of an acellular porcine annulus fibrosus scaffold. Cell Tissue Bank. 2017; 18(3):383–396. [PubMed: 28342099]
34. Mercuri JJ, Gill SS, Simionescu DT. Novel tissue-derived biomimetic scaffold for regenerating the human nucleus pulposus. J Biomed Mater Res Part A. 2011; 96A(2):422–435.
35. Chan LKY, Leung VYL, Tam V, Lu WW, Sze KY, Cheung KMC. Decellularized bovine intervertebral disc as a natural scaffold for xenogenic cell studies. Acta Biomater. 2013; 9(2): 5262–5272. [PubMed: 23000521]
36. Crapo PM, Gilbert TW, Badylak SF. An overview of tissue and whole organ decellularization processes. Biomaterials. 2011; 32(12):3233–3243. [PubMed: 21296410]
37. Gilbert T, Sellaro T, Badylak S. Decellularization of tissues and organs. Biomaterials. 2006; 27(19):3675–3683. [PubMed: 16519932]
38. Mercuri JJ, Patnaik S, Dion G, Gill SS, Liao J, Simionescu DT. Regenerative potential of decellularized porcine nucleus pulposus hydrogel scaffolds: stem cell differentiation, matrix remodeling, and biocompatibility studies. Tissue Eng Part A. 2013; 19(7–8):952–966. [PubMed: 23140227]
39. Liu Y, Fu S, Rahaman MN, Mao JJ, Bal BS. Native nucleus pulposus tissue matrix promotes notochordal differentiation of human induced pluripotent stem cells with potential for treating intervertebral disc degeneration. J Biomed Mater Res Part A. 2015; 103(3):1053–1059.
40. Roughley PJ. Biology of intervertebral disc aging and degeneration: involvement of the extracellular matrix. Spine (Phila Pa 1976). 2004; 29(23):2691–2699. [PubMed: 15564918]
41. Eyre D, Matsui Y, Wu J. Collagens of the disc. The Biology of the Intervertebral Disc. 1988:171–188.
42. Pearce RH, Grimmer BJ, Adams ME. Degeneration and the chemical composition of the human lumbar intervertebral disc. J Orthop Res. 1987; 5(2):198–205. [PubMed: 3572589]
43. Mwale F, Roughley P, Antoniou J. Distinction between the extracellular matrix of the nucleus pulposus and hyaline cartilage: a requisite for tissue engineering of intervertebral disc. Eur Cell Mater. 2004; 8:58–63-4. [PubMed: 15602703]
44. Iatridis JC, MacLean JJ, O'Brien M, Stokes IAF. Measurements of Proteoglycan and Water Content Distribution in Human Lumbar Intervertebral Discs. Spine (Phila Pa 1976). 2007; 32(14): 1493–1497. [PubMed: 17572617]
45. Mercuri JJ, Lovekamp JJ, Simionescu DT, Vyavahare NR. Glycosaminoglycan-targeted fixation for improved bioprosthetic heart valve stabilization. Biomaterials. 2007; 28(3):496–503. [PubMed: 17030363]
46. Yang S-H, Chen P-Q, Chen Y-F, Lin F-H. Gelatin/chondroitin-6-sulfate copolymer scaffold for culturing human nucleus pulposus cellsin vitro with production of extracellular matrix. J Biomed Mater Res Part B Appl Biomater. 2005; 74B(1):488–494.
47. Illien-Jünger S, Sedaghatpour DD, Laudier DM, Hecht AC, Qureshi SA, Iatridis JC. Development of a bovine decellularized extracellular matrix-biomaterial for nucleus pulposus regeneration. J Orthop Res. 2016; 34(5):876–888. [PubMed: 26509556]

Author Manuscript Author Manuscript Author Manuscript Author Manuscript

48. Mizuno H, Roy AK, Zaporojan V, Vacanti CA, Ueda M, Bonassar LJ. Biomechanical and biochemical characterization of composite tissue-engineered intervertebral discs. Biomaterials. 2006; 27(3):362–370. [PubMed: 16165204]

49. Schollum ML, Robertson PA, Broom ND. ISSLS Prize Winner: Microstructure and Mechanical Disruption of the Lumbar Disc Annulus. Spine (Phila Pa 1976). 2008; 33(25):2702–2710. [PubMed: 19002075]

50. Schollum ML, Robertson PA, Broom ND. A microstructural investigation of intervertebral disc lamellar connectivity: detailed analysis of the translamellar bridges. J Anat. 2009; 214(6):805–816. [PubMed: 19538627]

51. Han WM, Nerurkar NL, Smith LJ, Jacobs NT, Mauck RL, Elliott DM. Multi-scale Structural and Tensile Mechanical Response of Annulus Fibrosus to Osmotic Loading. Ann Biomed Eng. 2012; 40(7):1610–1621. [PubMed: 22314837]

52. Adam C, Rouch P, Skalli W. Inter-lamellar shear resistance confers compressive stiffness in the intervertebral disc: An image-based modelling study on the bovine caudal disc. J Biomech. 2015; 48(16):4303–4308. [PubMed: 26549764]

53. Urban JPG, Roberts S. Degeneration of the intervertebral disc. Arthritis Res Ther. 2003; 5(3):120–130. [PubMed: 12723977]

54. Chou AI, Reza AT, Nicoll SB. Distinct intervertebral disc cell populations adopt similar phenotypes in three-dimensional culture. Tissue Eng Part A. 2008; 14(12):2079–2087. [PubMed: 18636941]

55. Wilke HJ, Neef P, Caimi M, Hoogland T, Claes LE. New in vivo measurements of pressures in the intervertebral disc in daily life. Spine (Phila Pa 1976). 1999; 24(8):755–762. [PubMed: 10222525]

56. Johannessen W, Elliot D. Effects of degeneration on the biphasic material properties of human nucleus pulposus in confined compression. Spine (Phila Pa 1976). 2005; 30:E724–729. [PubMed: 16371889]

57. Nerurkar NL, Elliott DM, Mauck RL. Mechanical design criteria for intervertebral disc tissue engineering. J Biomech. 2010; 43(6):1017–1030. [PubMed: 20080239]

Author Manuscript Author Manuscript Author Manuscript Author Manuscript

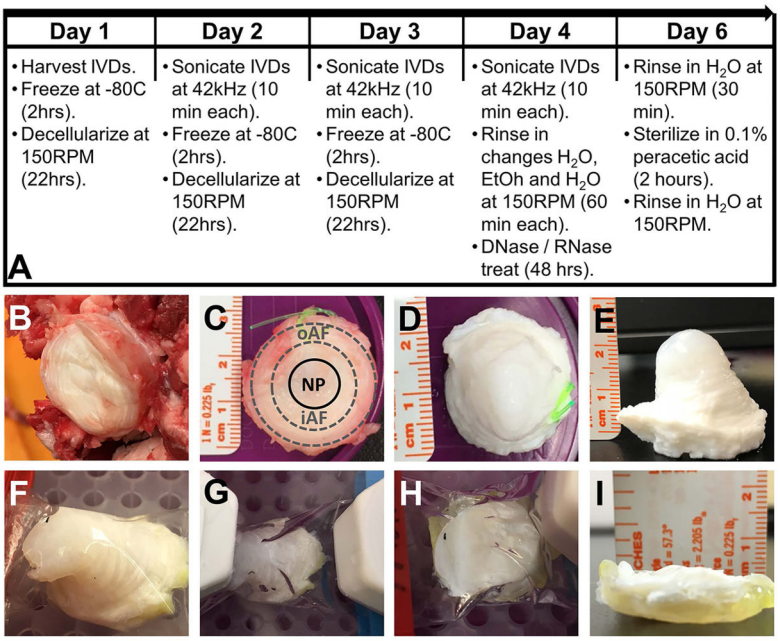

Figure 1.

Author Manuscript Author Manuscript Author Manuscript Author Manuscript

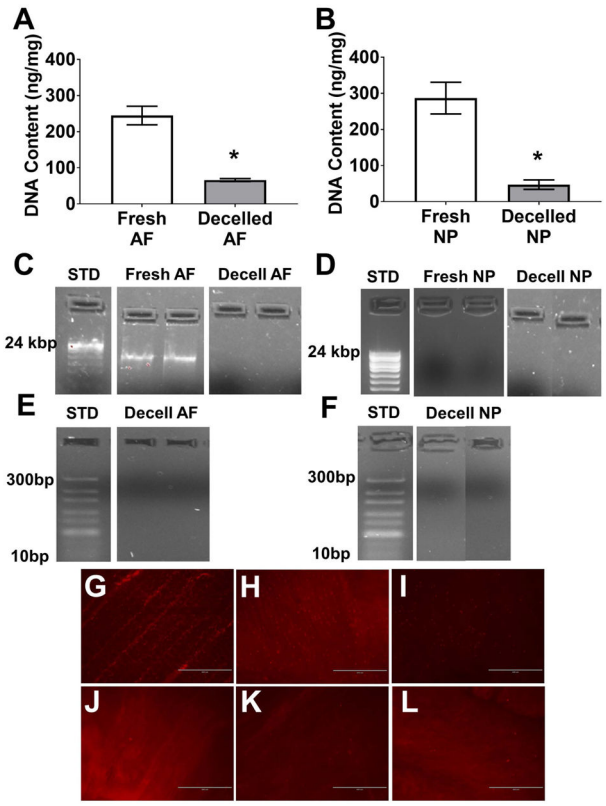

Figure 2.

Author Manuscript Author Manuscript Author Manuscript Author Manuscript

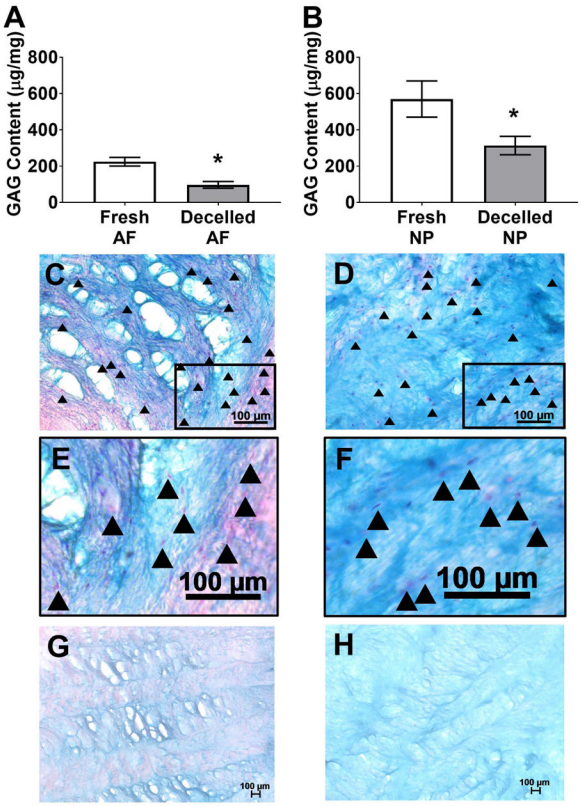

Figure 3.

Author Manuscript Author Manuscript Author Manuscript Author Manuscript

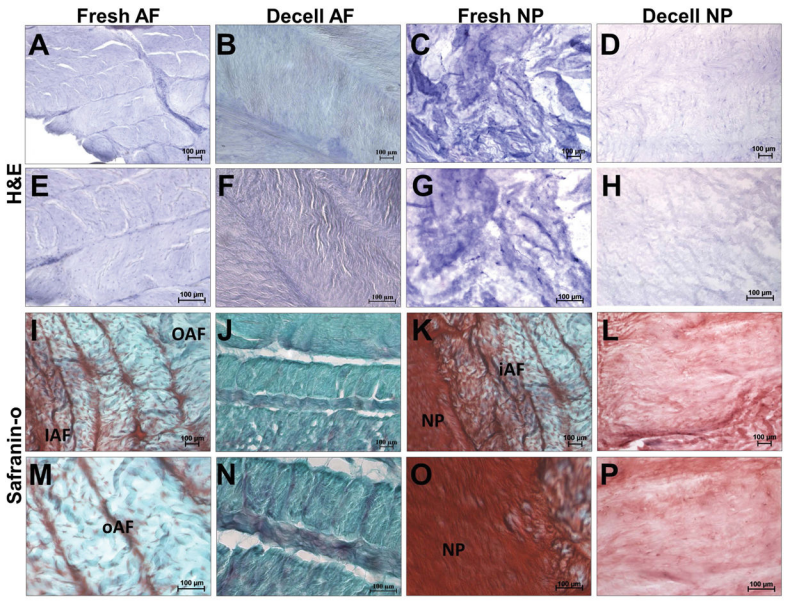

Figure 4.

Author Manuscript Author Manuscript Author Manuscript Author Manuscript

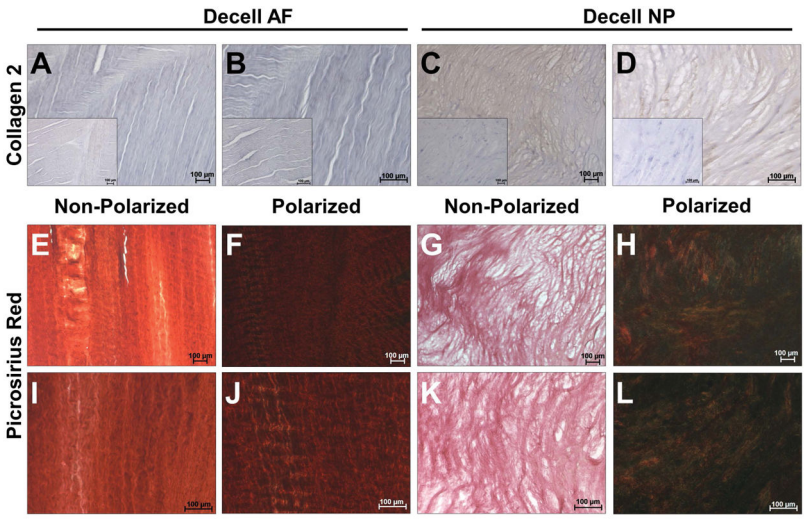

Figure 5.

Author Manuscript Author Manuscript Author Manuscript Author Manuscript

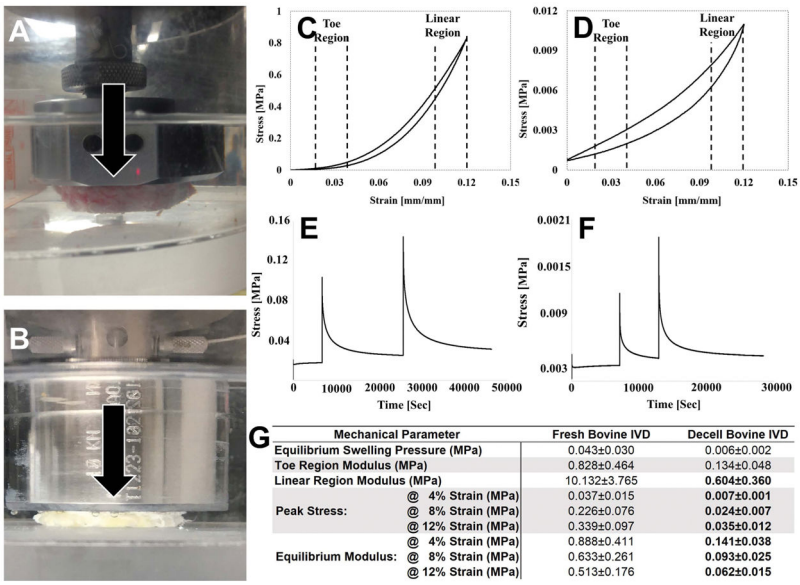

G

Mechanical Parameter		Fresh Bovine IVD	Decell Bovine IVD
Equilibrium Swelling Pressure (MPa)		0.043±0.030	0.006±0.002
Toe Region Modulus (MPa)		0.828±0.464	0.134±0.048
Linear Region Modulus (MPa)		10.132±3.765	**0.604±0.360**
Peak Stress:	@ 4% Strain (MPa)	0.037±0.015	**0.007±0.001**
	@ 8% Strain (MPa)	0.226±0.076	**0.024±0.007**
	@ 12% Strain (MPa)	0.339±0.097	**0.035±0.012**
Equilibrium Modulus:	@ 4% Strain (MPa)	0.888±0.411	**0.141±0.038**
	@ 8% Strain (MPa)	0.633±0.261	**0.093±0.025**
	@ 12% Strain (MPa)	0.513±0.176	**0.062±0.015**

Figure 6.